


Stearate-to-palmitate ratio modulates endoplasmic reticulum stress and cell apoptosis in non-B non-C hepatoma cells

Yasushi Shibasaki¹  | Makoto Horikawa^{2,3} | Koji Ikegami^{2,3} | Ryota Kiuchi¹ | Makoto Takeda¹ | Takanori Hiraide¹ | Yoshifumi Morita¹ | Hiroyuki Konno¹ | Hiroya Takeuchi¹ | Mitsutoshi Setou^{2,3} | Takanori Sakaguchi¹

¹Second Department of Surgery, Hamamatsu University School of Medicine, Hamamatsu, Shizuoka, Japan

²Department of Cellular & Molecular Anatomy, Hamamatsu University School of Medicine, Hamamatsu, Shizuoka, Japan

³International Mass Imaging Center, Hamamatsu University School of Medicine, Hamamatsu, Shizuoka, Japan

Correspondence

Takanori Sakaguchi, Second Department of Surgery, Hamamatsu University School of Medicine, Hamamatsu, Japan.
Email: saka1119@hama-med.ac.jp

Funding information

Grant-in-Aid for Scientific Research (No. 25462085) from the Ministry of Education, Culture, Sports, Science and Technology, Japan; Advanced Research and Development Programs for Medical Innovation (CREST) from the Japan Agency for Medical Research and Development; Imaging Platform supported by the Ministry of Education, Culture, Sports, Science and Technology (MEXT), Japan.

The increased prevalence of hepatocellular carcinoma (HCC) without viral infection, namely, NHCC, is a major public health issue worldwide. NHCC is frequently derived from non-alcoholic fatty liver (NAFL) and non-alcoholic steatohepatitis, which exhibit dysregulated fatty acid (FA) metabolism. This raises the possibility that NHCC evolves intracellular machineries to adapt to dysregulated FA metabolism. We herein aim to identify NHCC-specifically altered FA and key molecules to achieve the adaptation. To analyze FA, imaging mass spectrometry (IMS) was performed on 15 HCC specimens. The composition of saturated FA (SFA) in NHCC was altered from that in typical HCC. The stearate-to-palmitate ratio (SPR) was significantly increased in NHCC. Associated with the SPR increase, the ELOVL6 protein level was upregulated in NHCC. The knockdown of *ELOVL6* reduced SPR, and enhanced endoplasmic reticulum stress, inducing apoptosis of Huh7 and HepG2 cells. In conclusion, NHCC appears to adapt to an FA-rich environment by modulating SPR through *ELOVL6*.

KEYWORDS

ELOVL6, endoplasmic reticulum stress, hepatocellular carcinoma, non-alcoholic steatohepatitis, saturated fatty acid

1 | INTRODUCTION

Hepatocellular carcinoma (HCC) is the 5th most prevalent cancer and a leading cause of cancer death worldwide.¹ Although the most frequent etiology for HCC is viral infections such as the hepatitis B and C viruses, the prevalence of HCC without viral infection is increasing in Western countries² and Japan.³ In developed countries, 30%-40% of HCC cases arise from the liver without viral infection,⁴ suggesting a higher prevalence of metabolic syndrome with non-

alcoholic fatty liver disease (NAFLD) and non-alcoholic steatohepatitis (NASH) associated with the development of HCC.^{5,6}

Non-B non-C HCC (NHCC) and HCC with viral infection (VHCC) in advanced stages are currently treated in the same manner; however, their pathological features sometimes differ, such as the abundant deposition of triglycerides (TG) including a steatohepatitic appearance,⁷ which is commonly reported in NHCC. TG are composed of 3 fatty acids (FA) and glycerol, and their accumulation is the hallmark of NASH,^{8,9} resulting in hepatic dysfunction, such as

This is an open access article under the terms of the Creative Commons Attribution-NonCommercial License, which permits use, distribution and reproduction in any medium, provided the original work is properly cited and is not used for commercial purposes.

© 2018 The Authors. *Cancer Science* published by John Wiley & Sons Australia, Ltd on behalf of Japanese Cancer Association.

insulin resistance.^{10,11} Previous studies have demonstrated that hepatic TG themselves are not toxic and may protect the liver from FA-induced lipotoxicity,¹² but lipogenesis has an important role in cellular survival of HCC.¹³ However, the toxic effects of FA on hepatic cancer cells have not yet been examined in detail.

Saturated FA (SFA), including palmitate (C16:0; PA) and stearate (C18:0; SA), exert toxic effects on living cells by inducing endoplasmic reticulum (ER) stress,^{14,15} which leads to cell apoptosis. However, monounsaturated FA (MUFA), such as oleate (C18:1n9; OA), have been shown to alleviate SFA-induced deleterious effects.^{16,17} Although FA composition ratios such as the MUFA-to-SFA ratio are an important factor for cancer cell survival,^{18–20} limited information is currently available on SFA composition ratios. PA is synthesized through acetate polymerization in de novo lipogenesis.²¹ This long chain FA is then endogenously converted to SA by elongation of very long-chain fatty acids family member 6 (ELOVL6), or shifted to MUFA by stearoyl-CoA desaturase 1 (SCD-1) in the ER.²² ELOVL6 is a microsomal enzyme that alters the stearate-to-palmitate ratio (SPR) and has also been shown to mediate the progression of NASH.^{23–25}

We herein examined SPR in the cancerous parts (CA) and adjacent non-cancerous parenchyma (NC) of NHCC using matrix-assisted laser desorption/ionization imaging mass spectrometry (MALDI-IMS), and the relationship between SPR and the expression of ELOVL6 and SCD1. We also investigated the involvement of SPR in cancer progression using the hepatoma cell lines, Huh7 and HepG2, to clarify whether the results obtained may be applied to the development of therapeutic approaches for NHCC.

2 | MATERIALS AND METHODS

2.1 | Patients

This study was performed with the approval of the Institutional Ethics Committee of Hamamatsu University School of Medicine, and written informed consent was obtained from all patients. Fifteen HCC specimens were collected from patients undergoing hepatectomy for curative intent at Hamamatsu University Hospital between 2010 and 2012.

2.2 | Imaging mass spectrometry for human liver samples

Fifteen 10- μ m-thick frozen HCC specimens were placed on indium-tin oxide (ITO)-coated glass slides (Bruker Daltonics, Bremen, Germany). As a matrix, 5 mg/mL of 9-aminoacridine in 70% methanol (Merck, Darmstadt, Germany) was sprayed on the samples as previously described.^{26–29} Mass spectrometry (MS) was performed with a matrix-assisted laser desorption/ionization time-of-flight (MALDI-TOF/TOF) type instrument, the Ultraflex II (Bruker Daltonics). MS parameters were set to obtain the highest sensitivity with m/z values in the range of 200–1000 in the negative-ion mode. The automatic acquisition of spectra and reconstruction of ion images were performed using FlexImaging Software (Bruker Daltonics).

2.3 | Cell cultures

The human HCC cell lines Huh7 and HepG2 were maintained in DMEM (Invitrogen, Carlsbad, CA, USA) with 10% FBS, 100 U penicillin, and 0.1 mg/mL streptomycin at 37°C in a 5% CO₂ atmosphere.

2.4 | Immunoblotting

Rabbit polyclonal anti-ELOVL6 (Millipore Corporation, Billerica, MA, USA), mouse monoclonal anti-SCD1 (Abcam Tokyo, Japan), rabbit polyclonal anti-PARP, mouse monoclonal anti-caspase-3, rabbit polyclonal anti-cleaved caspase-3, rabbit monoclonal anti-PERK, rabbit monoclonal anti-phospho-PERK, and rabbit monoclonal anti-beta-actin for an internal standard (Cell Signaling Technology, Beverly, MA, USA) were used. Immunoreactive proteins were detected using an enhanced chemiluminescence system (GE Healthcare, Little Chalfont, Buckinghamshire, UK) and an LAS-3000 Luminescent Image Analyzer (Fujifilm, Tokyo, Japan).

2.5 | Quantitative RT-PCR

Total RNA was extracted from liver specimens and cells using ISOGEN (Nippon Gene, Tokyo, Japan) and the RNeasy Mini Kit (QIAGEN, Valencia, CA). mRNA were reverse transcribed to complementary DNA with the PrimeScript RT Reagent Kit (TAKARA BIO, Shiga, Japan). A quantitative RT-PCR analysis was performed with the Thermal Cycler Dice Real Time System Single (TAKARA) using SYBR green as a fluorophore. PCR primers were listed in Table S1. The expression of target mRNA was normalized to the expression level of cyclophilin A (*PPIA*).

2.6 | Immunofluorescence and a TUNEL assay for cell lines

Cells were fixed with 4% paraformaldehyde (PFA), washed with PBS, and immersed in PBS containing 5% goat serum and 0.1% Triton X-100 for blocking and permeabilization. A rabbit polyclonal anti-ELOVL6 antibody (1:300, Santa Cruz, CA, USA) and mouse monoclonal anti-Calnexin antibody (1:1000, Abcam Tokyo, Japan) were used as primary antibodies, followed by Alexa Fluor-conjugated secondary antibodies (1:1000, Abcam). In the TUNEL assay, an In Situ Apoptosis Detection Kit (Takara) was used according to the manufacturer's instructions. Samples were mounted in VECTASHIELD (Vector Laboratories, Burlingame, CA, USA), and fluorescence images were obtained using the confocal microscope FV1000 (OLYMPUS, Tokyo, Japan).

2.7 | Preparation of cells for imaging mass spectrometry

To perform IMS, 5×10^5 cells were incubated on ITO-coated slide glasses shielded by a rounded silicone rubber with a 15-mm pore for

10 hours. Cells were fixed with 4% PFA and washed with 150 mmol/L ammonium acetate 3 times. Slides were desiccated and cellular lipids were analyzed by Ultraflex II.

2.8 | Fatty acid preparation

Palmitate (PA) and stearate (SA) were purchased from Wako. Each FA stock solution was prepared as previously described.³⁰ Stock solutions of 100 mmol/L PA and SA dissolved in 0.1 mol/L sodium hydroxide were heated at 75°C, then added to DMEM containing 3% FA-free BSA (Sigma Aldrich, Munich, Germany) pre-heated at 55°C.³¹ The final concentrations of the working solutions were 2 mmol/L PA and SA. After filtration of the working solutions, they were diluted in DMEM for adjustments to the indicated concentrations.

2.9 | Modulation of ELOVL6 activity with siRNA

In the small interfering RNA inhibition assay, Huh7 and HepG2 cells were knocked down using Stealth RNAi (Invitrogen) against human *ELOVL6*, the sequences of which were 5'-CGCUGCUCUUCGAA-CUGCUGCUUUAU-3' and 5'-AUAAGCACCAGUUCG-AAGAGCACCG-3'. RNAi Negative Control Medium GC Duplex (Invitrogen) was used as a negative control. Cells were transfected with Lipofectamine RNAiMAX (Invitrogen) according to the manufacturer's instructions, and were incubated for 48 hours. Media were changed to DMEM containing 0.6 mmol/L PA, and cells were harvested 24 hours after the medium change.

2.10 | Cell proliferation assay

In knockdown experiments, 8×10^3 Huh7 cells and 5×10^3 HepG2 cells were plated on 96-well plates. Cell proliferation was measured 3 days after the completion of knockdown. The XTT Cell Proliferation Kit (Roche Applied Science, Penzberg, Germany) was used according to the manufacturer's instructions. The absorbance of live cells was measured with the Synergy HT Multi-Mode Microplate Reader (BioTek, Winooski, VT, USA).

2.11 | Statistical analysis

Statistical analyses were performed with SPSS Statistics software (version 21; SPSS, Chicago, USA). Results are expressed as the mean \pm SEM of at least 3 independent experiments. The χ^2 -test and Mann-Whitney *U*-test were used for analyses of clinical and histological features. The Wilcoxon signed-rank test was used for IMS and western blotting analyses. The *t* test and a univariate analysis of variance (ANOVA, Bonferroni procedure) were used to test for differences between 2 and more groups of samples, respectively. The relationship between SPR and *ELOVL6* expression in the immunoblot analysis was tested by Spearman's rank correlation coefficient. $P < .05$ was considered to indicate a significant difference.

3 | RESULTS

3.1 | NHCC patients were more likely to have steatosis in liver parenchyma

The clinicopathological features of 15 HCC patients are shown in Table 1. Macrovesicular steatosis and ballooning, which are commonly observed in steatohepatic HCC, were more frequently detected histologically in NHCC cancer (Figure S1).⁷ Five NHCC samples did not exhibit other historical hepatitis, such as autoimmune hepatitis.

3.2 | Saturated fatty acid signals identified by imaging mass spectrometry were altered in the cancerous parts of NHCC

Using IMS, the amounts of several molecules with different *m/z* values (mass numbers) were visualized in false colors for various sites, such as CA, adjacent NC, and fibrous and Glisson's capsules (Figure S2). Biomolecules detected using the negative ion mode of IMS

TABLE 1 Clinicopathological features of 15 patients with HCC

	NHCC	VHCC	P-value
Patient number	5	10	
Gender (M/F)	5/0	7/3	NS
Age (years)	71.2 \pm 2.85	68.3 \pm 2.35	NS
BMI (kg/m ²)	23.9 \pm 1.02	22.4 \pm 0.78	NS
Alcohol (y/n)	1/4	2/8	NS
Alb (g/dL)	4.3 \pm 0.10	4.2 \pm 0.10	NS
T. bil (mg/dL)	0.94 \pm 0.24	1.05 \pm 0.12	NS
AST (IU/L)	53.0 \pm 10.3	43.8 \pm 6.57	NS
ALT (IU/L)	49.2 \pm 12.5	38.0 \pm 9.88	NS
PT (%)	84.8 \pm 6.94	89.1 \pm 4.62	NS
ICG R15 (%)	17.8 \pm 9.49	18.0 \pm 3.85	NS
HbA1c (%)	6.08 \pm 0.25	5.76 \pm 0.23	NS
TG (mg/dL)	223.0 \pm 94.1	130.6 \pm 15.4	NS
T. chol (mg/dL)	176.8 \pm 11.4	174.3 \pm 12.0	NS
Tumor number (s/m)	3/2	7/3	NS
Tumor size (cm)	3.2 \pm 0.45	3.5 \pm 0.57	NS
Differentiation (w/m/p)	1/3/1	1/9/0	NS
Vessel invasion (y/n)	3/2	4/6	NS
Liver cirrhosis (y/n)	3/2	2/8	NS
Hepatitis activity score	1.6 \pm 0.40	1.5 \pm 0.17	NS
Fibrosis score	2.4 \pm 0.51	2.6 \pm 0.45	NS
UICC Stage (I/II/III)	1/1/3	1/5/4	NS

Alcohol, ethanol consumption of more than 20 g/day; BMI, body mass index; Differentiation, well-differentiated (w), moderately differentiated (m) and poorly differentiated (p); NHCC, HCC without viral infections; Tumor N, tumor number indicating a solitary (s) or multiple (m) tumors; VHCC, hepatocellular carcinoma (HCC) with viral infections. The clinical stage was assessed according to the UICC Classification.

for human liver samples are listed in Table 2. Signals conceivably derived from FA were also detected using the negative ion mode of IMS, as previously reported.^{32,33}

We then investigated SFA and MUFA compositions in 15 HCC samples. PA (C16:0), SA (C18:0) and C18-MUFA including both OA (C18:1n9) and VA (C18:1n7) were identified in HCC specimens (Figure 1A-C). Palmitoleate (C16:1) was not detectable in this experiment. The IMS analysis showed that PA levels were significantly lower, while SA levels were slightly higher in the CA than in the adjacent NC of NHCC, and this change was not observed in the CA or NC of VHCC (Figure 1A-C). Correspondingly, SPR was significantly elevated in the CA of NHCC, but not in the CA of VHCC (Figure 1D). C18-MUFA levels were higher in the CA than in the NC of both HCC, but a significant difference was only observed in the NC of VHCC. The C18-MUFA-to-SA ratio slightly increased in VHCC and NHCC (Figure 1E). SPR was more prominently and specifically altered in the CA of NHCC than in the CA of VHCC.

3.3 | Expression of ELOVL6, a stearate-to-palmitate ratio modulator, was upregulated in NHCC

ELOVL6 is an enzyme that synthesizes SA from PA and regulates cellular SPR. We analyzed ELOVL6 protein expression by immunoblotting and found that ELOVL6 protein levels were markedly higher in the CA than in the NC of NHCC (Figure 2A,B). However, significant alteration was not observed in ELOVL6 mRNA

expression (Figure S3A). In contrast, no significant differences were observed in ELOVL6 levels between the CA and NC of VHCC. We examined the protein level of stearoyl-CoA desaturase-1 (SCD-1) in NHCC and VHCC because SPR is also influenced by the desaturation of C16:0 and C18:0 by SCD-1. The results showed that the protein level of SCD-1 was significantly higher, without elevation of mRNA level (Figure S3B), in the CA than in the NC of VHCC and NHCC (Figure 2A,C), which is consistent with previous findings.³⁴

We then investigated the relationship between SPR and ELOVL6 protein levels. A correlation was observed between SPR and ELOVL6 protein levels in NHCC parenchyma ($r^2 = .60$, $P = .006$; Figure 2D) but not in VHCC (Figure 2E).

3.4 | Palmitate induced endoplasmic reticulum stress, whereas extrinsic stearate-to-palmitate modulation mitigated toxic effects in cell lines

To corroborate the importance of increases in SPR in the CA of NHCC, we examined the effects of extracellular FA supplementation on cell stress in cell line experiments. We used Huh7 and HepG2 cells, which are hepatoma cell lines without viral infections. IMS was performed on Huh7 and HepG2 cells and revealed that these cells have different FA compositions. PA (C16:0), SA (18:0) and C18-MUFA signals were easily detected in the 2 cell lines (Figure 3A). Endogenous SPR was higher in Huh7 than in HepG2 cells (Figure 3B). The expression levels of ELOVL6 and SCD mRNA were

TABLE 2 Molecule list identified by negative ion mode imaging mass spectrometry

Name	Symbol	m/z	Adduct	Formula	Signal intensity mean \pm SEM (%)			
					NHCC n = 5		VHCC n = 10	
					Non-cancer	Cancer	Non-cancer	Cancer
Palmitic acid	C16:0	255.3	M-H	C16H32O2	25.0 \pm 1.78	13.6 \pm 3.23*	20.7 \pm 3.09	19.6 \pm 3.42
Stearic acid	C18:0	283.3	M-H	C18H35O2	33.2 \pm 3.93	41.7 \pm 2.89	31.4 \pm 3.46	31.9 \pm 3.09
C-18MUFA (Oleic acid, vaccenic acid)	C18:1, n-9 C18:1, n-7	281.3	M-H	C18H34O2	12.3 \pm 1.28	21.4 \pm 6.67	12.9 \pm 2.14	17.8 \pm 4.04*
Linoleic acid	C18:2, n-6	279.3	M-H	C18H32O2	22.5 \pm 4.31	17.6 \pm 4.24	17.4 \pm 2.39	20.0 \pm 2.71
Arachidonic acid	C20:4 n-6	303.3	M-H	C20H32O2	3.9 \pm 0.48	4.2 \pm 0.29	5.1 \pm 0.65	7.3 \pm 1.73
Eicosapentaenoic acid	C20:5 n-3	301.3	M-H	C20H30O2	1.3 \pm 0.44	1.1 \pm 0.48	5.1 \pm 1.99	2.1 \pm 1.00
Docosahexaenoic acid	C22:6 n-3	327.3	M-H	C22H32O2	1.8 \pm 1.06	0.5 \pm 0.24*	7.3 \pm 6.50	1.2 \pm 0.72
C18:0/C16:0					1.32 \pm 0.13	3.55 \pm 0.60*	1.95 \pm 0.34	2.21 \pm 0.52
C18:1/C18:0					0.42 \pm 0.12	0.56 \pm 0.21	0.43 \pm 0.06	0.68 \pm 0.23
Phosphatidylinositol	PI 16:0/18:1	835.6	M-H	C43H81O13P	0.77 \pm 0.29	2.99 \pm 1.18	2.53 \pm 1.28	4.88 \pm 1.96
Phosphatidylinositol	PI 16:0/18:2	833.6	M-H	C43H79O13P	0.63 \pm 0.17	0.59 \pm 0.17	1.31 \pm 0.58	2.01 \pm 0.78
Phosphatidylinositol	PI 16:0/20:4	857.6	M-H	C45H79O13P	0.97 \pm 0.47	0.77 \pm 0.22	0.90 \pm 0.25	2.72 \pm 0.91
Phosphatidylinositol	PI 18:0/18:2	861.6	M-H	C45H83O13P	7.89 \pm 3.99	6.52 \pm 1.59	8.30 \pm 1.83	10.44 \pm 1.78
Phosphatidylinositol	PI 18:0/20:4	885.6	M-H	C47H83O13P	84.21 \pm 4.99	72.81 \pm 5.16	80.93 \pm 4.63	68.23 \pm 4.57*
Phosphatidylinositol	PI 18:0/20:3	888.6	M-H	C47H81O13P	1.65 \pm 0.37	8.21 \pm 5.11	1.86 \pm 0.26	4.66 \pm 1.30*
Phosphatidylinositol	PI 18:0/22:6	909.6	M-H	C49H83O13P	2.43 \pm 0.88	4.02 \pm 1.39	2.19 \pm 0.33	4.81 \pm 0.87*

*Means significantly different from adjacent non-cancerous parts, $P < .05$, the Wilcoxon signed-rank test.

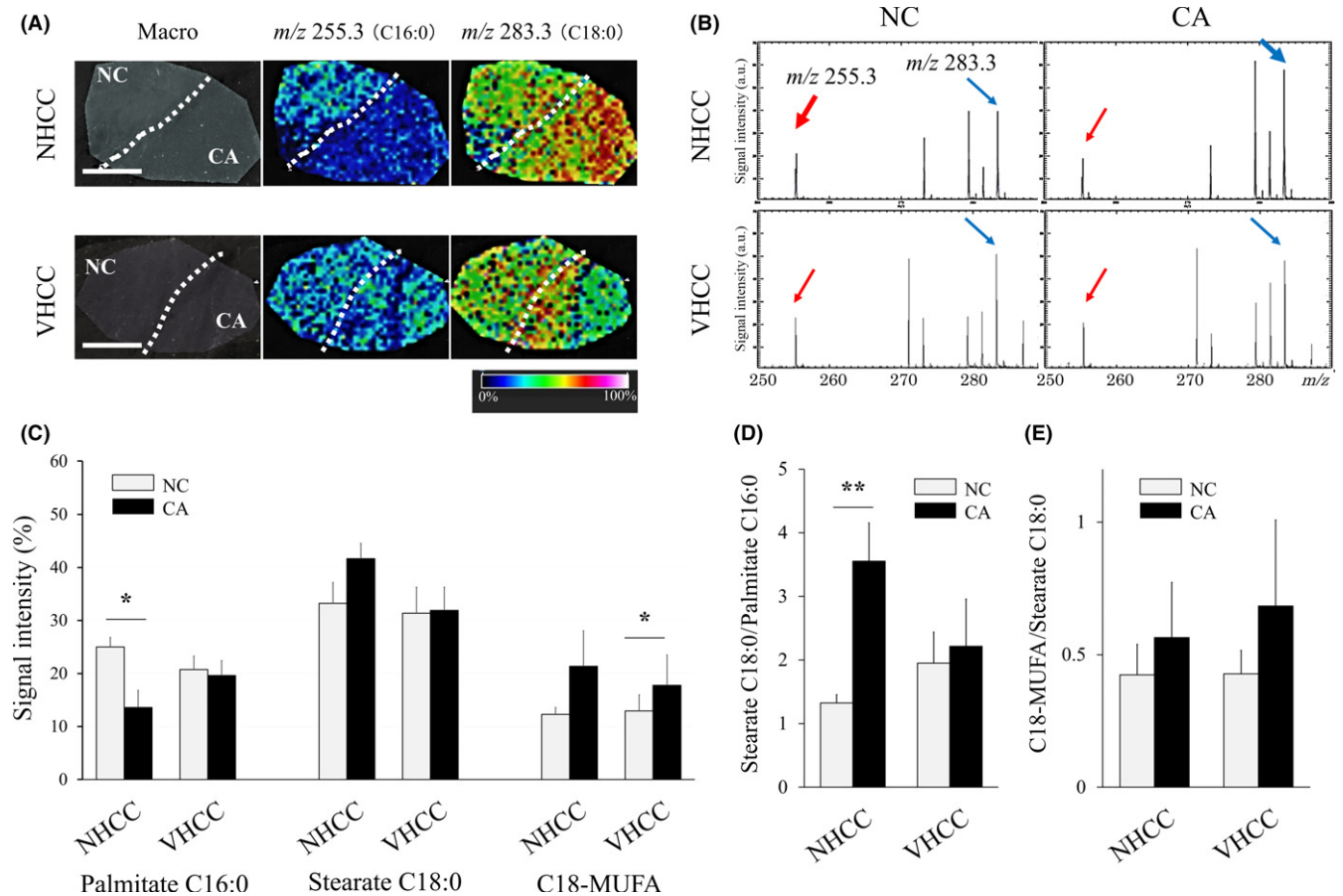


FIGURE 1 Saturated fatty acid signals identified by Imaging Mass Spectrometry in hepatocellular carcinoma (HCC). A, Typical reconstruction images acquired from imaging mass spectrometry (IMS) of NHCC (upper 3) and VHCC (lower 3 panels). White dotted lines indicate demarcations between cancerous parts (CA; right lower) and adjacent non-cancerous parenchyma (NC; left upper). Color variations were made according to the signal intensity of the substrate; blue, rarely existed; pink, abundant. The left panel shows a gross image of the specimen, and the middle and right panels show the abundance of PA and SA, respectively. The scale bar shows 1000 μ m. B, Signal intensities, acquired from IMS, of PA (red arrows) and SA (blue arrows) are shown in the upper left (NHCC-NC), upper right (NHCC -CA), lower left (VHCC-NC) and lower right panels (VHCC-CA). C, The signal intensity of saturated fatty acids (SFA) and monounsaturated fatty acids (MUFA) obtained from all samples, including NHCC ($n = 5$) and VHCC ($n = 10$), with comparisons between NC and CA. D, E, The stearate-to-palmitate ratio (SPR) (D) and C18-MUFA -to-stearate ratio (E) in the CA and NC of 5 NHCC and 10 VHCC resected specimens. * $P < .05$, ** $P < .01$ with the Wilcoxon signed-rank test

similar in the 2 cell lines (Figure 3C). ELOVL6 protein levels in Huh7 cells were also detected using immunofluorescence, which exhibited co-localization with calnexin, an ER marker (Figure 3D).

We then investigated changes in the ER stress response influenced by the modulation of exogenous SPR in vitro. Activating transcription factor 3 (ATF3), DNA-damage inducible transcript 3 (DDIT3) and splicing form of X-box binding protein 1 (XBP1) are ER stress markers.^{31,35,36} A previous study reported that PA upregulates these transcription factors and cell apoptosis.¹⁴ PA incubation (SPR = 0) upregulated the mRNA expression of ATF3, DDIT3 and XBP1s in a

dose-dependent manner in Huh7 (Figure 4A) and HepG2 cells (Figure S4A), as previously reported. In both cell lines, 600 μ mol/L SFA was sufficient to induce a stress response. Therefore, we examined the mechanisms by which SPR modulation affects the ER stress response in vitro. The expression of ATF3 and DDIT3 gradually decreased with increases in SPR from 0 (PA 600 μ mol/L alone) to 1 (PA 300 μ mol/L + SA 300 μ mol/L) (Huh7 in Figure 4A,B and HepG2 in Figure S4A,B). However, further increases in SPR were associated with counter effects, particularly in Huh7 cells (Figure 4B, compared with HepG2 data in Figure S4B). Consistent with the stronger mRNA

FIGURE 3 Fatty acid profile of hepatoma cell lines, Huh7 and HepG2. A, imaging mass spectrometry (IMS) of fatty acids in Huh7 (upper) and HepG2 cells (lower). Red arrows show palmitate (PA) (C16:0) and blue arrows are stearate (SA) (C18:0). B, Stearate-to-palmitate ratio (SPR) under normal conditions in Huh7 (red) and HepG2 cells (green). C, Relative expression of the mRNA of ELOVL6 and SCD in Huh7 (red) and HepG2 cells (green). D, Representative immunofluorescence images of ELOVL6 (green) and calnexin (endoplasmic reticulum [ER] marker, red) and the nucleus (blue) of Huh7 cells. The scale bar shows 20 μ m

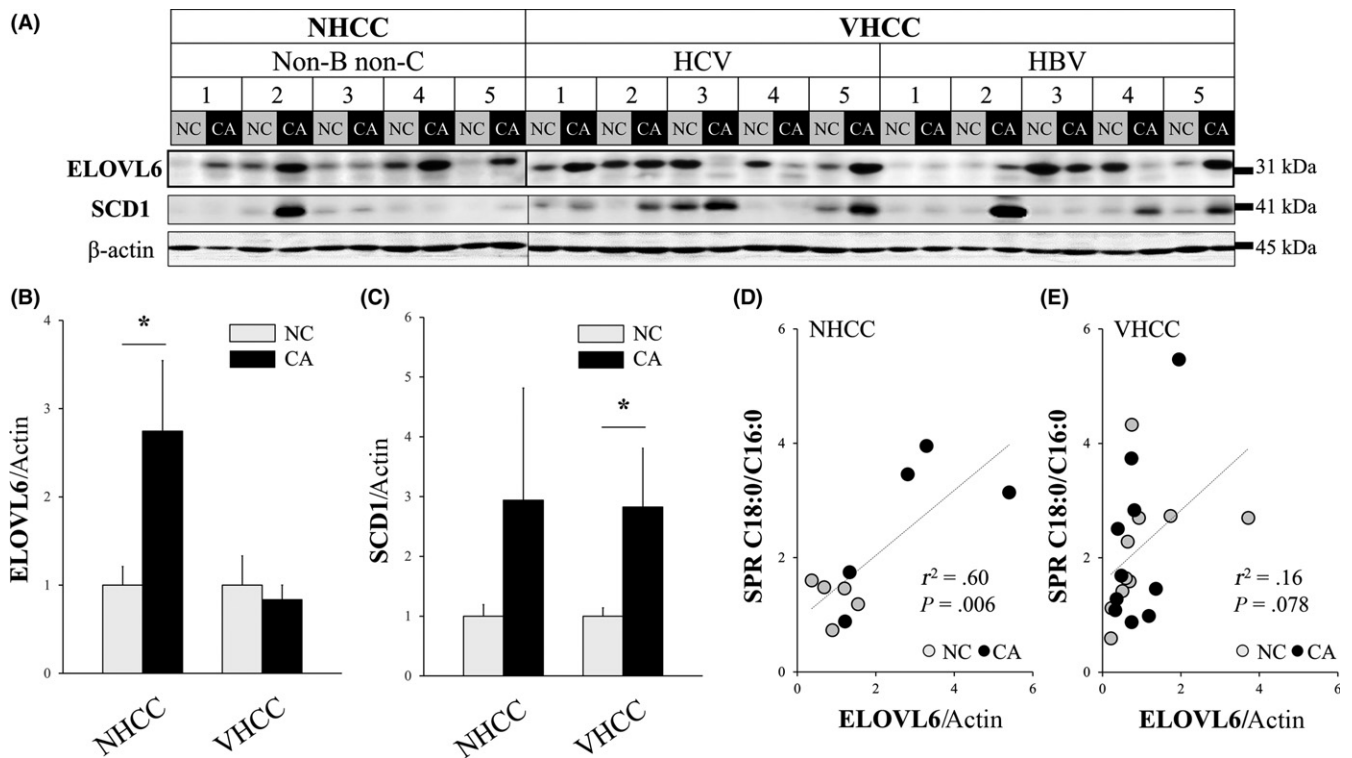
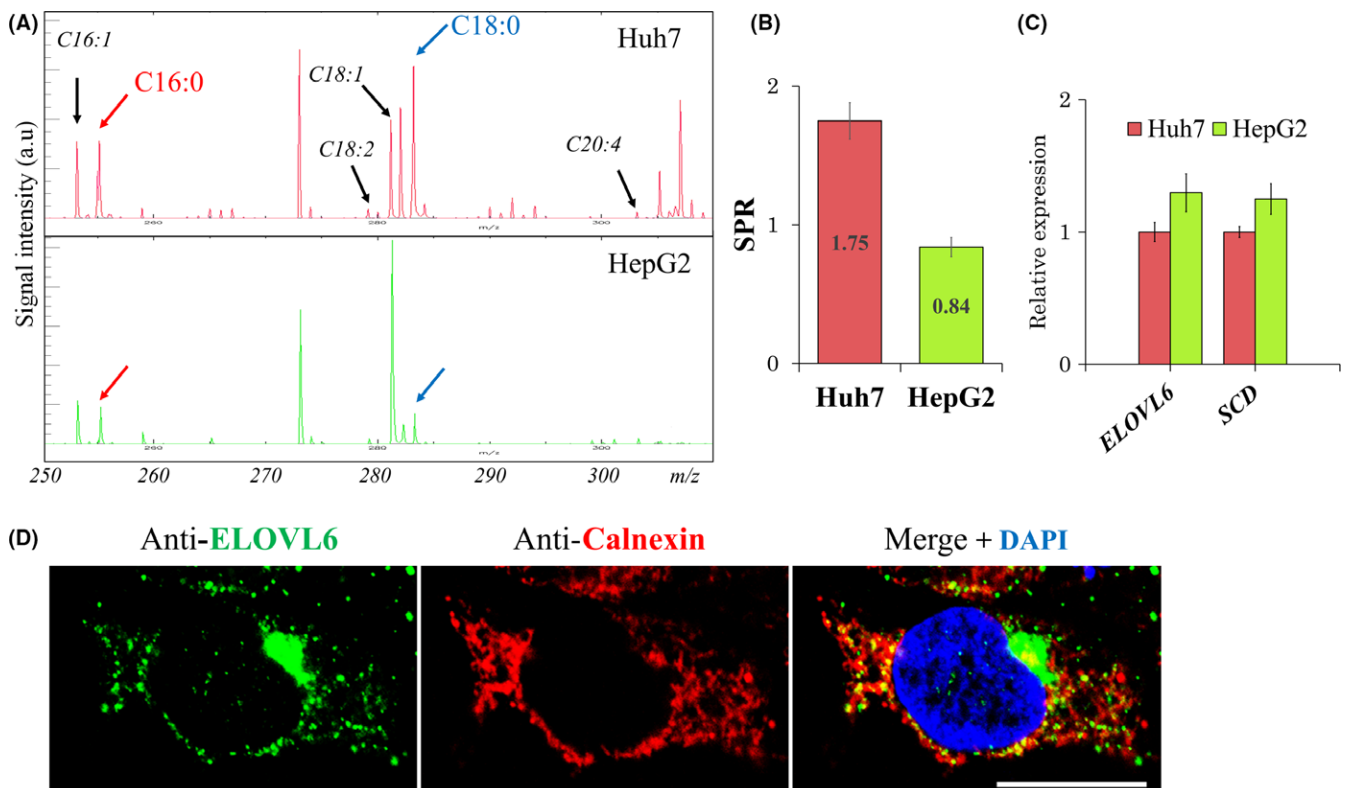


FIGURE 2 Immunoblot analysis for human liver samples and its relationship with the stearate-to-palmitate ratio (SPR). A, Immunoblot analysis of ELOVL6 and SCD1 in 15 HCC samples in the cancerous parts (CA) and adjacent non-cancerous parts (NC). B, C, Densitometry of ELOVL6 (B) and SCD1 (C) expression normalized by beta-actin, and normalized to that of NC. * $P < .05$ with the Wilcoxon signed-rank test. D, E, The relationship between SPR assessed by imaging mass spectrometry (IMS) and ELOVL6 expression in NHCC (D) and VHCC (E). Statistical analyses were performed with Spearman's rank correlation coefficient



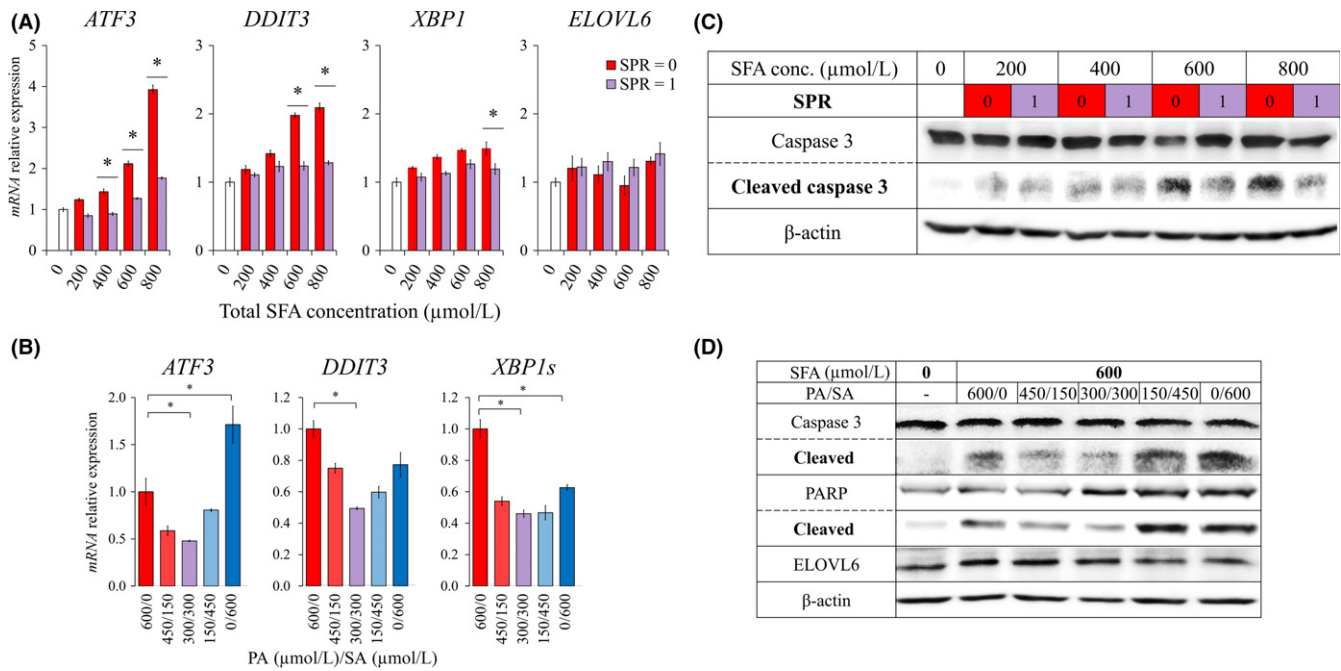


FIGURE 4 Endoplasmic reticulum (ER) stress mediated by extracellular fatty acid supplementation in Huh7 cells. A, Quantitative PCR for the mRNA of ER stress-associated transcription factors and *ELOVL6* after a 24-hours incubation with saturated fatty acids (SFA). SFA concentrations were modified from 0 to 800 μmol/L with an altered stearate-to-palmitate ratio (SPR). SPR = 0 at 800 μmol/L indicates a treatment with 800 μmol/L palmitate (PA), while SPR = 1 at 800 μmol/L means a treatment with 400 μmol/L each of PA and stearate (SA). * $P < .05$, significant difference in expression between SPR = 0 and SPR = 1 using the paired t test. *ATF3*, activating transcription factor 3; *DDIT3*, DNA-damage inducible transcript 3; and *XBP1*, splicing form of X-box binding protein 1. B, mRNA expression of ER stress-associated transcription factors after 24-hours SFA incubation at a concentration of 600 μmol/L with various SPR (0/600; SPR = 0, 150/450, 300/300; SPR = 1, 450/150 and 600/0) in Huh7 cells. * $P < .05$ (Bonferroni procedure). C, D, Immunoblot analysis of caspase-3, poly ADP-ribose polymerase (PARP), *ELOVL6*, and beta-actin with the modulation of SFA concentrations and SPR for 24 hours

expression of ER stress-associated transcription factors, cleaved caspase 3 and cleaved poly ADP-ribose polymerase (PARP) protein (a specific 85-kDa form observed during apoptosis)³⁷ were downregulated together with SPR modulation from 0 to 1 in the immunoblotting analysis (Huh7 in Figure 4C,D and HepG2 in Figure S4C,D). No alterations were observed in *ELOVL6* mRNA or protein expression levels between SPR = 0 and SPR = 1 24 hours after the treatment with SFA (Figure 4C,D and Figure S4C,D). These results suggest that lipotoxic effects are altered not only by the concentration of SFA but also by SPR modulation.

3.5 | Silencing *ELOVL6* lowered the stearate-to-palmitate ratio and increased the endoplasmic reticulum stress response

We speculated that SPR modulation, from 0 to 1, may be parallel to the process of FA elongation regulated by *ELOVL6*. Therefore, we examined whether *ELOVL6* silencing decreases SPR. In Huh7 cells, endogenous SPR was decreased to approximately 50% by *ELOVL6* silencing, irrespective of extracellular PA supplementation (Figure 5A,B), along with reductions in *ELOVL6* mRNA and protein levels (Figure 5C,D). Similar to the results shown in Figure 4, extracellular PA supplementation upregulated the mRNA of the ER stress-associated transcriptional factors, *ATF3* and *DDIT3* (Figure 5C, compare siControl with siControl+PA). The silencing of

ELOVL6 also increased these mRNA (Figure 5C). *ATF3* mRNA was upregulated further by *ELOVL6* silencing plus extracellular PA supplementation.

The phosphorylated form of the RNA protein kinase RNA-like endoplasmic reticulum kinase (PERK), an ER stress sensor, is known as a pro-apoptotic factor.^{38,39} In the immunoblotting analysis, we found that *ELOVL6* silencing increased phosphorylated PERK cooperatively with extracellular PA supplementation. We showed that cleaved caspase-3 and PARP were upregulated additively by *ELOVL6* silencing and extracellular PA supplementation (Figure 5D).

Similar results were also obtained for HepG2 cells (Figure S5), indicating that cancer cells escape PA-induced lipotoxicity by SPR modulation via FA elongation by *ELOVL6*.

3.6 | Cell survival and lipid accumulation caused by silencing *ELOVL6* and the palmitate treatment

The results of the immunoblotting analysis indicated that reductions in SPR induce cellular apoptosis. Therefore, we performed a TUNEL assay to clarify whether SPR modulation induces apoptosis in Huh7 cells. *ELOVL6* silencing significantly decreased cell numbers, but increased TUNEL-positive cell numbers (Figure 6A-C). *ELOVL6* silencing reduced lipid droplets in Huh7 cells (Figure 6A). Cell proliferation was also suppressed by *ELOVL6* silencing

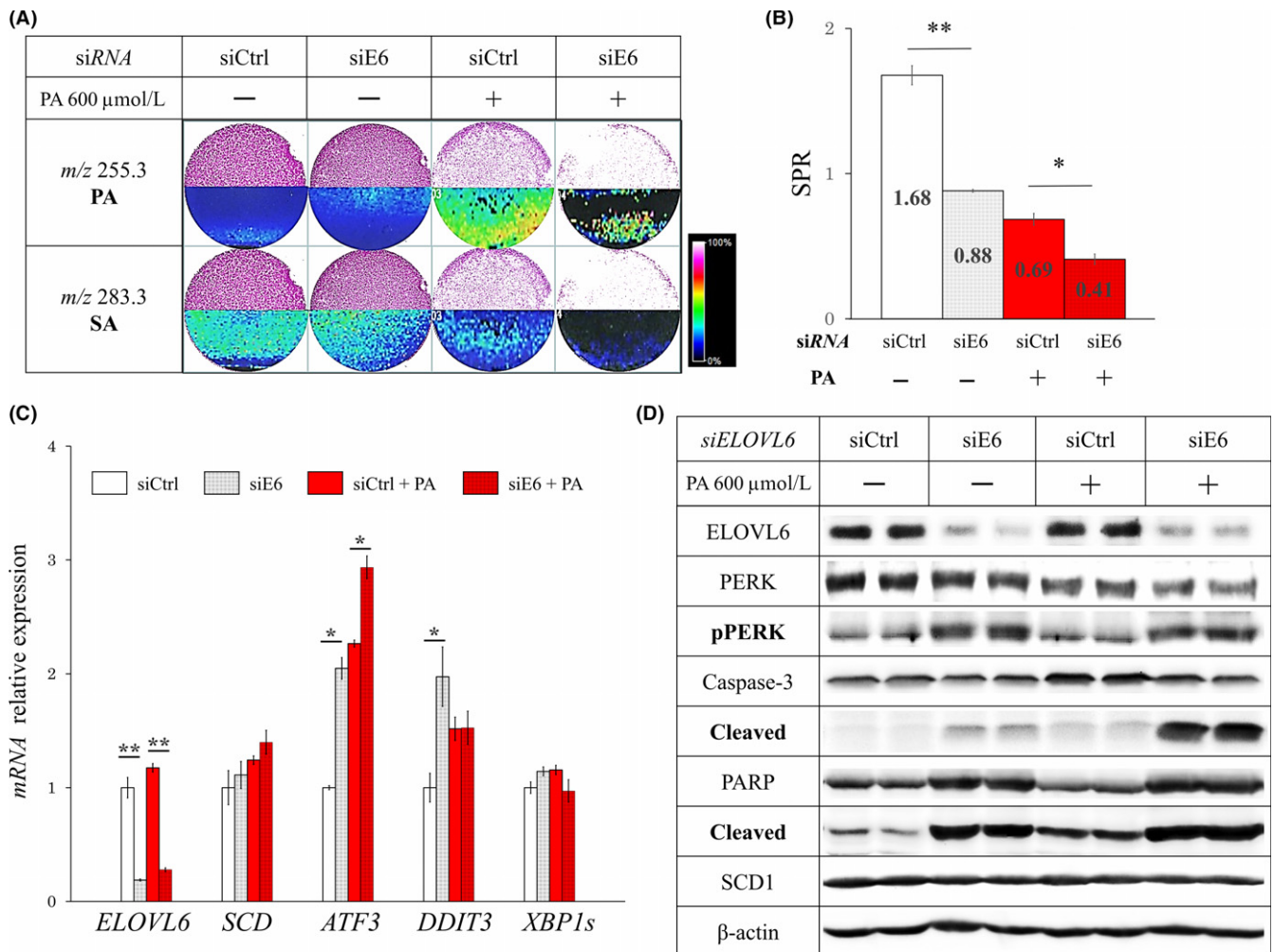


FIGURE 5 Silencing *ELOVL6* decreased the stearate-to-palmitate ratio (SPR) and increased the endoplasmic reticulum (ER) stress response in Huh7 cells. A, The reconstruction image of IMS for Huh7 cells after a 48-hours transfection with siRNA and a 24-hours incubation in the absence or presence of palmitate (PA, 600 $\mu\text{mol/L}$). The 4 upper and lower panels show images of PA (*m/z* 255.3) and SA (*m/z* 283.3) contents, respectively. siCtrl, transfected by control siRNA; siE6, transfected by *ELOVL6*-specific siRNA. B, stearate-to-palmitate ratio (SPR) calculated with imaging mass spectrometry (IMS) results. * $P < .05$, ** $P < .01$ with the paired *t* test. C, Expression levels of mRNA by qPCR. siCtrl (open bar), transfected by control siRNA, and siE6 (dotted bar), transfected by *ELOVL6*-specific siRNA. Red bars (+PA) show the results obtained after a further 24-hours supplementation with 600 $\mu\text{mol/L}$ PA. * $P < .05$, ** $P < .01$ with the paired *t* test. D, Immunoblot analysis of *ELOVL6*, protein kinase RNA-like endoplasmic reticulum kinase (PERK) and its phosphorylated form, caspase-3 and its cleaved form, poly ADP-ribose polymerase (PARP) and its cleaved form, SCD1, and beta-actin

(Figure 6D). Supplementation with 600 $\mu\text{mol/L}$ extracellular PA aggravated these effects (Figure 6A-D).

The same results were observed in HepG2 cells (Figure S6). The only difference between Huh7 and HepG2 cells was the absence of lipid droplets when incubated with siControl in the absence of extracellular PA.

4 | DISCUSSION

An increase in morbidity associated with HCC derived from aberrant lipid metabolism, such as NAFL and NASH, is a major public health issue worldwide. Although preventive approaches for HCC through the consumption of MUFA have been reported,^{40,41} the

therapeutic capability of FA for NHCC remains unclear. In the present study, PA concentrations decreased in the CA of NHCC, resulting in the upregulation of SPR. *ELOVL6* is known to be upregulated in NASH patients,⁴² and the protein expression of this enzyme was elevated in CA of NHCC in the present study. Furthermore, a correlation was observed between *ELOVL6* expression and SPR. Because low SPR induces severe lipotoxicity by PA, leading to cell apoptosis via ER stress in hepatoma cell lines, our results suggest that moderate elevations in SPR may avoid cell death and support cancer cell survival.

The results of our *in vitro* experiments demonstrated that endogenous SPR was distinct in the 2 cell lines examined, suggesting that the appropriate SPR differs in each cell or organ. Huh7 is a hepatocellular carcinoma cell derived from a liver tumor⁴³ and

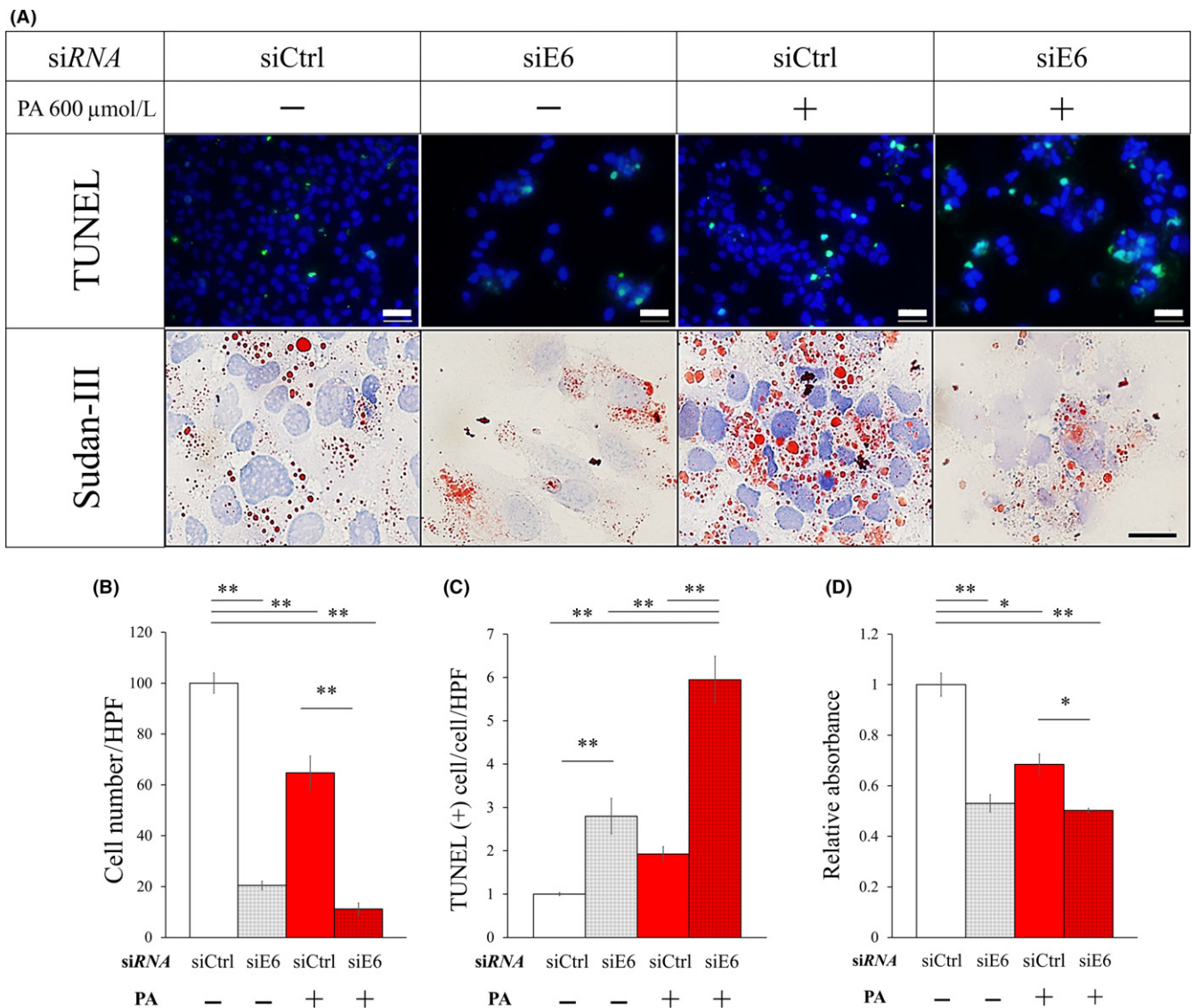


FIGURE 6 Cell survival and proliferation after siRNA transfection with or without a palmitate treatment in Huh7 cells. A, Images of the TUNEL assay after a 48-hours transfection with siRNA and further 24-hours incubation in the absence or presence of palmitate (palmitate, 600 $\mu\text{mol/L}$). The scale bar shows 50 μm (4 upper panels). The 4 lower panels show oil staining images by Sudan III. The scale bar shows 20 μm . B, C, The total cell count in a high-power field (HPF; 400-fold magnification) (B) and TUNEL-positive cell count per total cell count (C) in each condition. D, Cell proliferation measured by the XTT assay under each condition. * $P < .05$, ** $P < .01$, using the Bonferroni procedure

HepG2 is a hepatoblastoma cell line derived from liver tissue.⁴⁴ Therefore, Huh7 may be more similar to the CA of NHCC and a suitable model for the study of NHCC. Huh7 cells had high endogenous SPR, which may have induced sensitivity to high concentrations of SA. These results support previous findings showing that ELOVL6 enhanced deleterious effects on pancreatic β -cells.^{31,45}

However, these results reflect the short-term effects of SPR in vitro, and SPR is also influenced by other factors such as PA synthase; that is, acetyl-CoA carboxylase (ACC) and FA synthase (FAS),⁴⁶ β -oxidation⁴⁷ and food intake. Previous studies demonstrated that SPR decreased with the upregulated expression of ELOVL6 in NASH patients.^{42,48} These controversial results suggest

that SPR is also influenced by other factors and that certain feedback mechanisms regulate SPR in the long term.

Palmitate and SA-induced lipotoxicity in the liver has been reported in previous studies.⁴⁹⁻⁵¹ We herein demonstrated SFA-induced toxicity in vitro; however, these deleterious effects were altered by changing exogenous SPR under the same total SFA concentration. Free PA and SA are activated by acyl-CoA synthetase into fatty acyl-CoA, which are the primary substrates for energy use via β -oxidation and the synthesis of TG and phospholipids.^{52,53} We previously reported that lysophosphatidylcholine acyltransferase-1 (LPCAT1), which specifically incorporates SFA into membrane phosphatidylcholine,⁵⁴ regulates the progression of HCC.^{55,56} Previous studies have demonstrated that elevated membrane saturation

caused inflammation and altered signal transduction.⁵⁷⁻⁵⁹ In TG synthesis, saturated fatty acyl-CoA is incorporated into lipid droplets,^{60,61} with substrate specificities.⁶²⁻⁶⁴ This selective usage of SFA may be one of the mechanisms underlying cancer cell survival.

In conclusion, NHCC and hepatoma cell lines may maintain an appropriate SPR to attenuate SFA-induced lipotoxicity by modulating the ER stress response. Therefore, the modulation of SPR has potential as a therapeutic approach for NHCC.

CONFLICT OF INTEREST

The authors have no conflict of interest.

ORCID

Yasushi Shibasaki  <http://orcid.org/0000-0002-9286-2534>

REFERENCES

- Siegel R, Naishadham D, Jemal A. Cancer statistics, 2012. *CA Cancer J Clin.* 2012;62:10-29.
- Ascha MS, Hanouneh IA, Lopez R, Tamimi TA, Feldstein AF, Zein NN. The incidence and risk factors of hepatocellular carcinoma in patients with nonalcoholic steatohepatitis. *Hepatology.* 2010;51:1972-1978.
- Tokushige K, Hashimoto E, Kodama K. Hepatocarcinogenesis in non-alcoholic fatty liver disease in Japan. *J Gastroenterol Hepatol.* 2013;28(Suppl 4):88-92.
- El-Serag HB. Hepatocellular carcinoma. *N Engl J Med.* 2011;365:1118-1127.
- Duan XY, Zhang L, Fan JG, Qiao L. NAFLD leads to liver cancer: do we have sufficient evidence? *Cancer Lett.* 2014;345:230-234.
- Alzahrani B, Iseli TJ, Hebbard LW. Non-viral causes of liver cancer: does obesity led inflammation play a role? *Cancer Lett.* 2014;345:223-229.
- Salomao M, Yu WM, Brown RS Jr, Emond JC, Lefkowitz JH. Steatohepatitic hepatocellular carcinoma (SH-HCC): a distinctive histological variant of HCC in hepatitis C virus-related cirrhosis with associated NAFLD/NASH. *Am J Surg Pathol.* 2010;34:1630-1636.
- Charlton M. Nonalcoholic fatty liver disease: a review of current understanding and future impact. *Clin Gastroenterol Hepatol.* 2004;2:1048-1058.
- Walenbergh SM, Shiri-Sverdlov R. Cholesterol is a significant risk factor for non-alcoholic steatohepatitis. *Expert Rev Gastroenterol Hepatol.* 2015;9:1343-1346.
- Kumashiro N, Erion DM, Zhang D, et al. Cellular mechanism of insulin resistance in nonalcoholic fatty liver disease. *Proc Natl Acad Sci USA.* 2011;108:16381-16385.
- Khavandi M, Duarte F, Ginsberg HN, Reyes-Soffer G. Treatment of dyslipidemias to prevent cardiovascular disease in patients with type 2 diabetes. *Curr Cardiol Rep.* 2017;19:7.
- Yamaguchi K, Yang L, McCall S, et al. Inhibiting triglyceride synthesis improves hepatic steatosis but exacerbates liver damage and fibrosis in obese mice with nonalcoholic steatohepatitis. *Hepatology.* 2007;45:1366-1374.
- Feng S, Han M, Zhou L, et al. NS5A/BP37 inhibits liver cancer by impeding lipogenesis and cholesterologenesis. *Cancer Sci.* 2017;108:12-22.
- Hotamisligil GS. Endoplasmic reticulum stress and atherosclerosis. *Nat Med.* 2010;16:396-399.
- Marwarha G, Claycombe K, Schommer J, Collins D, Ghribi O. Palmitate-induced endoplasmic reticulum stress and subsequent C/EBP α homologous protein activation attenuates leptin and insulin-like growth factor 1 expression in the brain. *Cell Signal.* 2016;28:1789-1805.
- Akazawa Y, Cazanave S, Mott JL, et al. Palmitoleate attenuates palmitate-induced Bim and PUMA up-regulation and hepatocyte lipoapoptosis. *J Hepatol.* 2010;52:586-593.
- Liu F, Huang H, Gong Y, Li J, Zhang X, Cao Y. Evaluation of in vitro toxicity of polymeric micelles to human endothelial cells under different conditions. *Chem Biol Interact.* 2017;263:46-54.
- Mason P, Liang B, Li L, et al. SCD1 inhibition causes cancer cell death by depleting mono-unsaturated fatty acids. *PLoS ONE.* 2012;7:e33823.
- Chen L, Ren J, Yang L, et al. Stearoyl-CoA desaturase-1 mediated cell apoptosis in colorectal cancer by promoting ceramide synthesis. *Sci Rep.* 2016;6:19665.
- Huang J, Fan XX, He J, et al. SCD1 is associated with tumor promotion, late stage and poor survival in lung adenocarcinoma. *Oncotarget.* 2016;7:39970-39979.
- Aarsland A, Wolfe RR. Hepatic secretion of VLDL fatty acids during stimulated lipogenesis in men. *J Lipid Res.* 1998;39:1280-1286.
- Matsuzaka T, Shimano H, Yahagi N, et al. Crucial role of a long-chain fatty acid elongase, Elovl6, in obesity-induced insulin resistance. *Nat Med.* 2007;13:1193-1202.
- Muir K, Hazim A, He Y, et al. Proteomic and lipidomic signatures of lipid metabolism in NASH-associated hepatocellular carcinoma. *Can Res.* 2013;73:4722-4731.
- Kessler SM, Simon Y, Gemperlein K, et al. Fatty acid elongation in non-alcoholic steatohepatitis and hepatocellular carcinoma. *Int J Mol Sci.* 2014;15:5762-5773.
- Kuba M, Matsuzaka T, Matsumori R, et al. Absence of Elovl6 attenuates steatohepatitis but promotes gallstone formation in a lithogenic diet-fed Ldlr(-/-) mouse model. *Sci Rep.* 2015;5:17604.
- Kubo A, Ohmura M, Wakui M, et al. Semi-quantitative analyses of metabolic systems of human colon cancer metastatic xenografts in livers of superimmunodeficient NOG mice. *Anal Bioanal Chem.* 2011;400:1895-1904.
- Hirano-Sakamaki W, Sugiyama E, Hayasaka T, Ravid R, Setou M, Taki T. Alzheimer's disease is associated with disordered localization of ganglioside GM1 molecular species in the human dentate gyrus. *FEBS Lett.* 2015;589:3611-3616.
- Morita Y, Ikegami K, Goto-Inoue N, et al. Imaging mass spectrometry of gastric carcinoma in formalin-fixed paraffin-embedded tissue microarray. *Cancer Sci.* 2010;101:267-273.
- Kurabe N, Hayasaka T, Ogawa M, et al. Accumulated phosphatidylcholine (16:0/16:1) in human colorectal cancer; possible involvement of LPCAT4. *Cancer Sci.* 2013;104:1295-1302.
- Cousin SP, Hugl SR, Wrede CE, Kajio H, Myers MG Jr, Rhodes CJ. Free fatty acid-induced inhibition of glucose and insulin-like growth factor I-induced deoxyribonucleic acid synthesis in the pancreatic beta-cell line INS-1. *Endocrinology.* 2001;142:229-240.
- Green CD, Olson LK. Modulation of palmitate-induced endoplasmic reticulum stress and apoptosis in pancreatic beta-cells by stearoyl-CoA desaturase and Elovl6. *Am J Physiol Endocrinol Metab.* 2011;300:E640-E649.
- Hayasaka T, Goto-Inoue N, Zaima N, et al. Imaging mass spectrometry with silver nanoparticles reveals the distribution of fatty acids in mouse retinal sections. *J Am Soc Mass Spectrom.* 2010;21:1446-1454.
- Waki M, Sugiyama E, Kondo T, Sano K, Setou M. Nanoparticle-assisted laser desorption/ionization for metabolite imaging. *Methods Mol Biol.* 2015;1203:159-173.
- Huang GM, Jiang QH, Cai C, Qu M, Shen W. SCD1 negatively regulates autophagy-induced cell death in human hepatocellular

- carcinoma through inactivation of the AMPK signaling pathway. *Cancer Lett.* 2015;358:180-190.
35. Bensellam M, Maxwell EL, Chan JY, et al. Hypoxia reduces ER-to-Golgi protein trafficking and increases cell death by inhibiting the adaptive unfolded protein response in mouse beta cells. *Diabetologia.* 2016;59:1492-1502.
 36. Pavlovsky AA, Boehning D, Li D, Zhang Y, Fan X, Green TA. Psychological stress, cocaine and natural reward each induce endoplasmic reticulum stress genes in rat brain. *Neuroscience.* 2013;246:160-169.
 37. Tewari M, Quan LT, O'Rourke K, et al. Yama/PPP32 beta, a mammalian homolog of CED-3, is a CrmA-inhibitable protease that cleaves the death substrate poly(ADP-ribose) polymerase. *Cell.* 1995;81:801-809.
 38. Hetz C. The unfolded protein response: controlling cell fate decisions under ER stress and beyond. *Nat Rev Mol Cell Biol.* 2012;13:89-102.
 39. Tao SC, Yuan T, Rui BY, Zhu ZZ, Guo SC, Zhang CQ. Exosomes derived from human platelet-rich plasma prevent apoptosis induced by glucocorticoid-associated endoplasmic reticulum stress in rat osteonecrosis of the femoral head via the Akt/Bad/Bcl-2 signal pathway. *Theranostics.* 2017;7:733-750.
 40. Sawada N, Inoue M, Iwasaki M, et al. Consumption of n-3 fatty acids and fish reduces risk of hepatocellular carcinoma. *Gastroenterology.* 2012;142:1468-1475.
 41. Lai KK, Kweon SM, Chi F, et al. Stearoyl-CoA desaturase promotes liver fibrosis and tumor development in mice via a Wnt positive-signaling loop by stabilization of low-density lipoprotein receptor-related proteins 5 and 6. *Gastroenterology.* 2017;152:1477-1491.
 42. Matsuzaka T, Atsumi A, Matsumori R, et al. Elovl6 promotes nonalcoholic steatohepatitis. *Hepatology.* 2012;56:2199-2208.
 43. Nakabayashi H, Taketa K, Miyano K, Yamane T, Sato J. Growth of human hepatoma cells lines with differentiated functions in chemically defined medium. *Cancer Res.* 1982;42:3858-3863.
 44. Lopez-Terrada D, Cheung SW, Finegold MJ, Knowles BB. Hep G2 is a hepatoblastoma-derived cell line. *Human Pathol.* 2009;40:1512-1515.
 45. Tang N, Matsuzaka T, Suzuki M, et al. Ablation of Elovl6 protects pancreatic islets from high-fat diet-induced impairment of insulin secretion. *Biochem Biophys Res Commun.* 2014;450:318-323.
 46. Bassilian S, Ahmed S, Lim SK, Boros LG, Mao CS, Lee WN. Loss of regulation of lipogenesis in the Zucker diabetic rat. II. Changes in stearate and oleate synthesis. *Am J Physiol Endocrinol Metab.* 2002;282:E507-E513.
 47. Wen H, Ting JP, O'Neill LA. A role for the NLRP3 inflammasome in metabolic diseases-did Warburg miss inflammation? *Nat Immunol.* 2012;13:352-357.
 48. Yamada K, Mizukoshi E, Sunagozaka H, et al. Characteristics of hepatic fatty acid compositions in patients with nonalcoholic steatohepatitis. *Liver Int.* 2014;35:582-590.
 49. Wei Y, Wang D, Topczewski F, Pagliassotti MJ. Saturated fatty acids induce endoplasmic reticulum stress and apoptosis independently of ceramide in liver cells. *Am J Physiol Endocrinol Metab.* 2006;291:E275-E281.
 50. Nivala AM, Reese L, Frye M, Gentile CL, Pagliassotti MJ. Fatty acid-mediated endoplasmic reticulum stress in vivo: differential response to the infusion of soybean and lard oil in rats. *Metabolism.* 2013;62:753-760.
 51. Wei Y, Wang D, Gentile CL, Pagliassotti MJ. Reduced endoplasmic reticulum luminal calcium links saturated fatty acid-mediated endoplasmic reticulum stress and cell death in liver cells. *Mol Cell Biochem.* 2009;331:31-40.
 52. Lewin TM, Kim JH, Granger DA, Vance JE, Coleman RA. Acyl-CoA synthetase isoforms 1, 4, and 5 are present in different subcellular membranes in rat liver and can be inhibited independently. *J Biol Chem.* 2001;276:24674-24679.
 53. Yan S, Yang XF, Liu HL, Fu N, Ouyang Y, Qing K. Long-chain acyl-CoA synthetase in fatty acid metabolism involved in liver and other diseases: an update. *World J Gastroenterol.* 2015;21:3492-3498.
 54. Nakanishi H, Shindou H, Hishikawa D, et al. Cloning and characterization of mouse lung-type acyl-CoA:lysophosphatidylcholine acyltransferase 1 (LPCAT1). Expression in alveolar type II cells and possible involvement in surfactant production. *J Biol Chem.* 2006;281:20140-20147.
 55. Morita Y, Sakaguchi T, Ikegami K, et al. Lysophosphatidylcholine acyltransferase 1 altered phospholipid composition and regulated hepatoma progression. *J Hepatol.* 2013;59:292-299.
 56. Uehara T, Kikuchi H, Miyazaki S, et al. Overexpression of lysophosphatidylcholine acyltransferase 1 and concomitant lipid alterations in gastric cancer. *Ann Surg Oncol.* 2016;23(Suppl 2):S206-S213.
 57. Holzer RG, Park EJ, Li N, et al. Saturated fatty acids induce c-Src clustering within membrane subdomains, leading to JNK activation. *Cell.* 2011;147:173-184.
 58. Rong X, Albert CJ, Hong C, et al. LXRs regulate ER stress and inflammation through dynamic modulation of membrane phospholipid composition. *Cell Metab.* 2013;18:685-697.
 59. Boss M, Newbatt Y, Gupta S, Collins I, Brune B, Namgaladze D. AMPK-independent inhibition of human macrophage ER stress response by AICAR. *Sci Rep.* 2016;6:32111.
 60. Agarwal AK, Garg A. Congenital generalized lipodystrophy: significance of triglyceride biosynthetic pathways. *Trends Endocrinol Metab.* 2003;14:214-221.
 61. Rutkowski JM, Stern JH, Scherer PE. The cell biology of fat expansion. *J Cell Biol.* 2015;208:501-512.
 62. Ahmadian M, Duncan RE, Jaworski K, Sarkadi-Nagy E, Sul HS. Triacylglycerol metabolism in adipose tissue. *Future Lipidol.* 2007;2:229-237.
 63. Li C, Li L, Lian J, et al. Roles of Acyl-CoA: diacylglycerol acyltransferases 1 and 2 in triacylglycerol synthesis and secretion in primary hepatocytes. *Arterioscler Thromb Vasc Biol.* 2015;35:1080-1091.
 64. Kuo A, Lee MY, Sessa WC. Lipid droplet biogenesis and function in the endothelium. *Circ Res.* 2017;120:1289-1297.

SUPPORTING INFORMATION

Additional Supporting Information may be found online in the supporting information tab for this article.

How to cite this article: Shibasaki Y, Horikawa M, Ikegami K, et al. Stearate-to-palmitate ratio modulates endoplasmic reticulum stress and cell apoptosis in non-B non-C hepatoma cells. *Cancer Sci.* 2018;109:1110-1120. <https://doi.org/10.1111/cas.13529>